Nanoscale Res Lett (2009) 4:518–525
DOI 10.1007/s11671-009-9274-1

NANO EXPRESS

Synthesis and Characterization of Rutile TiO_2 Nanopowders Doped with Iron Ions

Nadica D. Abazović · Luciana Mirenghi · Ivana A. Janković · Nataša Bibić · Daniela V. Šojić · Biljana F. Abramović · Mirjana I. Čomor

Received: 8 December 2008 / Accepted: 8 February 2009 / Published online: 28 February 2009

Abstract Titanium dioxide nanopowders doped with different amounts of Fe ions were prepared by coprecipitation method. Obtained materials were characterized by structural (XRD), morphological (TEM and SEM), optical (UV/vis reflection and photoluminescence, and Raman), and analytical techniques (XPS and ICP-OES). XRD analysis revealed rutile crystalline phase for doped and undoped titanium dioxide obtained in the same manner. Diameter of the particles was 5–7 nm. The presence of iron ions was confirmed by XPS and ICP-OES. Doping process moved absorption threshold of TiO_2 into visible spectrum range. Photocatalytic activity was also checked. Doped nanopowders showed normal and up-converted photoluminescence.

Keywords Titanium dioxide · Rutile · Doping · Characterization

Introduction

Since its commercial production in the early 20th century, titanium dioxide (TiO_2) has been widely used as a pigment [1] and in sunscreens [2, 3], paints [4], ointments, toothpaste [5], etc. In 1972, Fujishima and Honda [6–8] discovered the phenomenon of photocatalytic splitting of water on a TiO_2 electrode under ultraviolet (UV) light. Since then, enormous efforts have been devoted to the research of TiO_2 material, which has led to many promising applications in areas ranging from photovoltaics and photocatalysis to photo/electrochromics and sensors [9–12]. These applications can be roughly divided into "energy" and "environmental" categories, many of which depend not only on the properties of the TiO_2 material itself but also on the modifications of the TiO_2 material host (e.g., with inorganic and organic dyes) and on the interactions of TiO_2 materials with the environment [13].

An exponential growth of research activities has been seen in nanoscience and nanotechnology in the past decades [14–18]. New physical and chemical properties emerge when the size of the material becomes smaller and smaller, and down to the nanometer scale. Among the unique properties of nanomaterials, the movement of electrons and holes in semiconductor nanomaterials is primarily governed by the well-known quantum confinement and the transport properties related to phonons and photons are largely affected by the size and geometry of the materials [14–17]. The specific surface area and surface-to-volume ratio increases dramatically as the size of a material decreases [14, 19]. The high surface area brought about by the small particle size is beneficial to many TiO_2-based devices, as it facilitates reaction/interaction between the devices and the interacting media, which mainly occurs on the surface or at the interface and strongly depends on the surface area of the material. Thus, the performance of TiO_2-based devices is largely influenced by the sizes of the TiO_2 building units, apparently at the nanometer scale.

N. D. Abazović · I. A. Janković · N. Bibić · M. I. Čomor (✉)
Vinča Institute of Nuclear Sciences, P.O. Box 522, Belgrade 11000, Serbia
e-mail: mirjanac@vinca.rs; mirjanac@vin.bg.ac.yu

L. Mirenghi
ENEA, UTS MAT, Brindisi Research Centre, S.S.7 Appia, Brindisi 72100, Italy

D. V. Šojić · B. F. Abramović
Department of Chemistry, Faculty of Sciences, University of Novi Sad, Trg D. Obradovića 3, Novi Sad 21000, Serbia

Titanium dioxide can be obtained in three crystalline phases: anatase, rutile, and brookite. The most stable phase is rutile and it is usually obtained after annealing at temperature above 500 °C [20]. TiO_2 is transparent normally in the visible light region; its band gap is 3.0 eV for rutile and 3.2 eV for anatase crystalline phase. By doping or sensitization, it is possible to improve the optical activity of TiO_2 and to move its absorption threshold into the visible light region.

The subject of this work is the synthesis by low temperature coprecipitation method of Fe-doped TiO_2 nanopowders and their characterization. Several concentrations of Fe ions were implied. Detailed characterization was conducted and photodegradation of mecoprop was chosen as a probe reaction for evaluation of photocatalytic activity of prepared samples. The relationship between optical properties (PL) and photoactivity of samples is discussed.

Experimental Section

All chemicals used were of p.a. purity and were used without further purification. Triply distilled water was used for aqueous solutions.

Fe-doped TiO_2 powders were prepared by a modified synthetic procedure of Abazović et al. [21]. An appropriate amount of $FeCl_3$ (Aldrich) was dissolved in 200 mL of triply distilled water. Then, 5 mL of $TiCl_4$ (Fluka) prechilled to −20 °C was added dropwise into solution containing $FeCl_3$ under stirring. After 2 h of stirring at room temperature, the obtained dispersions were heated and kept at 50 °C for 16 h with constant stirring. The resulting precipitates were dialyzed against water until test reaction for Cl^- ions was negative and subsequently dried in vacuum at 40 °C. Pure TiO_2 powder was synthesized in the same manner, without $FeCl_3$ in the reaction solution.

The obtained powders were characterized by several techniques. For UV/vis spectrometry a Perkin–Elmer λ-35 spectrophotometer, equipped with reflectance accessory and referenced with $BaSO_4$, was used. Photoluminescence was measured using a Perkin–Elmer LS-3b instrument. Raman spectra were obtained using a Raman system R-2001™.

The X-ray diffraction measurements of the powders were performed on a Philips PW1710 diffractometer.

Microstructural characterization of the iron ions doped TiO_2 nanopowders was carried out on a Philips EM-400 transmission electron microscope operated at 100 kV and on a Cambridge 250MKIII scanning electron microscope. Samples for TEM analysis were dispersed in methanol, ultrasonicated for 1 h and deposited on C-coated Cu grids. Samples for SEM were deposited on carbon tapes.

The X-ray photoelectron spectroscopy (XPS) measurements were carried out on a VG Scientific ESCALAB 210 spectrometer using non-monochromatic MgK_α radiation. The calibration of peak position was made using the Ag $3d_{5/2}$ line at 368.26 eV of a standard silver foil, used as a reference sample. It was in situ sputtered with argon ions in order to remove the surface oxide and acquire a clean reference spectrum. We used C1s to calibrate the peak positions after experimental acquisitions, because on the surface region carbon was well detected and unequivocally associated to adventitious carbon (for air exposure of the samples) expected at 285 eV of binding energy [22].

Chemical quantitative analysis was performed by inductively coupled plasma optical emission spectroscopy (Spectroflame ICP, 2.5 kW, 27 MHz). ICP-OES analysis was performed by measuring the intensity of radiation of the specific wavelengths emitted by each element. The samples dispersed in liquid were introduced into the plasma as aerosol, where they were vaporized, atomized, and excited.

Photocatalytic degradation was carried out in a cell made of Pyrex glass (total volume of ca. 40 mL, liquid layer thickness 35 mm), with a plain window on which the light beam was focused, equipped with a magnetic stirring bar and a water circulating jacket. A 125 W medium-pressure mercury lamp (Philips, HPL-N, emission bands in the UV region at 304, 314, 335, and 366 nm, with maximum emission at 366 nm), together with an appropriate concave mirror, was used as the radiation source.

Experiments were carried out using 20 mL of the solution of mecoprop (2.7 mmol dm^{-3}) and 40 mg of catalyst. Herbicide mecoprop (RS-2-(4-chloro-otolyloxy) propionic acid, $C_{10}H_{11}ClO_3$) was chosen as a model compound of a photodegradable organic waste substance in water because of its worldwide use for the selective control of many annual and some perennial weeds and because it is the herbicide most often found in drinking water [23, 24].The aqueous suspensions were sonicated in the dark for 15 min before illumination, to make the photocatalyst particles uniform and attain adsorption equilibrium. The suspensions thus obtained were thermostated at 40 ± 0.5 °C, in a stream of O_2 and then irradiated. During the irradiation, the mixtures were stirred at a constant speed.

Photocatalytic activity was checked on a spectrophotometer (Secomam anthelie Advanced 2). Namely, 0.25 cm^3 aliquots of the samples were taken at different illumination times and diluted to 10.00 cm^3 with double distilled water. The suspensions containing photocatalyst were filtered through Millipore (Milex-GV, 0.22 μm) membrane filters and spectra were recorded on a spectrophotometer. Kinetics of the aromatic ring degradation was monitored at 228 nm.

Results and Discussion

The crystal phase of the prepared powders was rutile as can be seen in Fig. 1. All XRD peaks ((110), (101), (111), (210), (211), and (220)) correspond to rutile crystal structure [25]. The diameter of the particles was calculated using the Scherrer diffraction formula, relating the diffraction angular width (β) at the half height of the (101) diffraction peak, to the domain size:

$$D = \frac{k\lambda}{\beta \cos\theta} \quad (1)$$

where k is a geometrical factor taken to be 0.89, $\lambda = 1.541$ Å is the X-ray wavelength, and θ is the diffraction angle of the most prominent peak for rutile structure ($2\theta \sim 27.4°$). We found that Fe-doped TiO_2 crystal domains are in the range from 5 to 7 nm in diameter. X-ray structural analysis of doped samples showed that the samples had typical peaks of rutile structure without any detectable dopant related peaks. The dopant ions may have been moved either into interstitial positions or substitutional sites of the TiO_2 nanocrystal structure, or their concentration was too low to be detected.

Raman spectra of our samples are consistent with XRD data and suggested pure rutile structure as can be seen in Fig. 2. According to literature data, rutile features in the Raman spectra are bands at 241, 444, and 607 cm^{-1} [26]. Our pure TiO_2 and doped TiO_2 powders have bands at 435 and 600 cm^{-1}. Band at 241 cm^{-1} is not visible in our spectra, due to technical limitations of the Raman device. The Raman peak broadening and small frequency blue-shifting compared to literature [26] might be attributed to variation of particle sizes or the stoichiometry in the samples (oxygen vacancies) [27, 28].

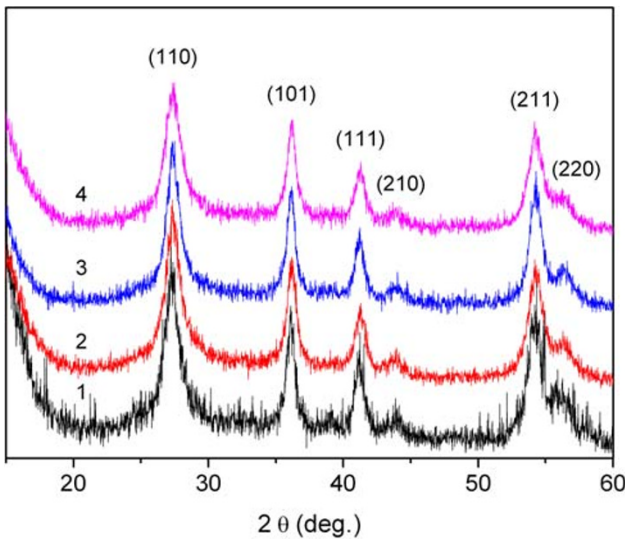

Fig. 1 XRD pattern of pure and Fe-doped TiO_2 nanopowders with atomic percent (stoichiometric concentration) of dopant ions: 1.0%; 2.5%; 3.10%; and 4.20%

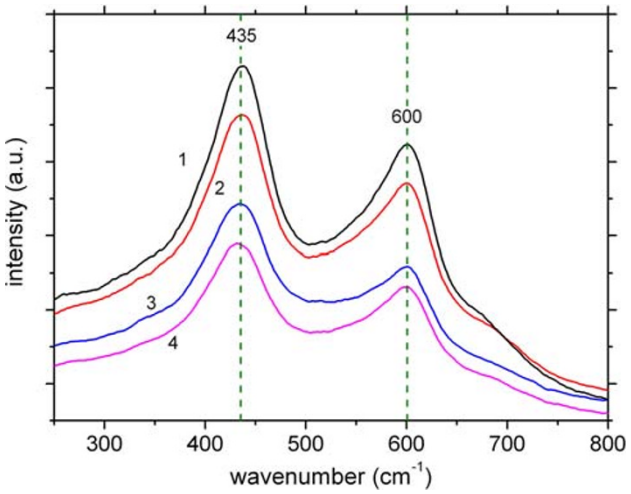

Fig. 2 Raman spectra of pure and Fe-doped TiO_2 nanopowders with atomic percent (stoichiometric concentration) of dopant ions: 1.0%; 2.5%; 3.10%; and 4.20%

In Fig. 3 a typical TEM images of pure (A) and Fe-doped (B) TiO_2 powder nanoparticles can be seen. For both materials flower-like agglomerates with diameters in the size range from 100 to 150 nm can be observed. Flower-like agglomerates consist of nanorods with 5–10 nm diameters. Similar morphology was observed after prolonged aging at room temperature of titania particles prepared by acidic hydrolysis of titanium tetrabutoxide in reverse micelles [25]. In Fig. 3b spherical nanoparticles with 5–10 nm diameters can also be seen. The formation of well-defined TiO_2 nanorods most likely can be explained by the prolonged aging at elevated temperature. This is in agreement with literature data concerning hydrothermal synthesis of TiO_2 rods [21, 29, 30].

Diameters are in good agreement with the diameters obtained from XRD measurements using the Scherrer diffraction formula. Similar TiO_2 morphology was observed for all dopant concentrations.

SEM images of the Fe-doped TiO_2 agglomerates are presented in Fig. 4. The sizes of agglomerates were of broad distribution and could not be determined exactly from the SEM images. It is obvious that the particles agglomerated during synthesis and drying, but they could be re-dispersed in appropriate solvent using an ultrasonic bath. Samples for SEM were prepared by direct deposition of powder on carbon tapes so agglomerates were observable. Agglomerates of TiO_2 particles doped with 10 at.% of Fe have smaller sizes (Fig. 4a) than agglomerates of TiO_2 particles doped with 20 at.% of Fe, but their size distribution was narrower (Fig. 4b).

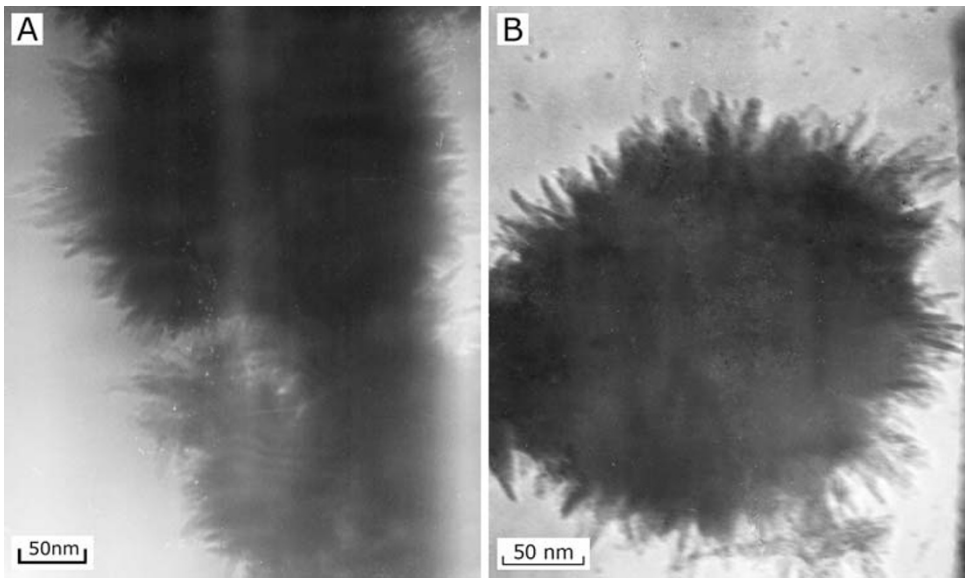

Fig. 3 Typical TEM images of pure TiO_2 (**a**) and 10 at.% Fe–TiO_2 (**b**)

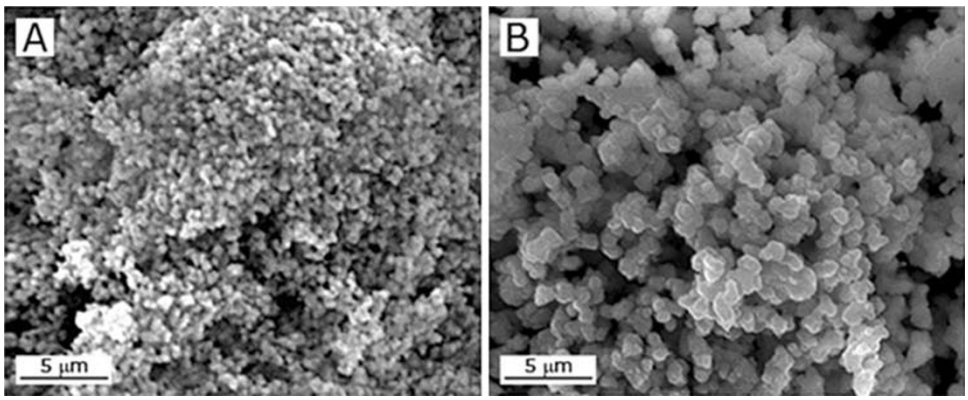

Fig. 4 Typical SEM images of TiO_2 powders doped with 10 at.% Fe (**a**) and 20 at.% Fe (**b**)

In order to reveal the presence of iron ions in our samples, which was not confirmed by XRD measurements, and to define oxidation state of Fe ions, we have examined three areas of the XPS spectrum of our samples: the Ti 2p region between 455 and 470 eV (Fig. 5a), the O 1s region between 525 and 535 eV (Fig. 5b) and the Fe $2p_{3/2}$ region near 710 eV (Fig. 5c). It must be noted that in all spectra peak at around 284.6 eV was found (not presented in Fig. 5a), corresponding to carbon impurities, arising probably from the background of XPS test or the residual precursors. The Ti $2p_{1/2}$ and Ti $2p_{3/2}$ spin-orbital splitting photoelectrons for all samples are located at binding energies of 464.6 and 458.9 eV, respectively, as can be seen in Fig. 5a. These data are in excellent agreement with data obtained by Zhu et al. [31]. It seems that these energies are not affected by doping with iron ions. Although, due to the low concentration of iron, the shift of Ti 2p peaks could have been below the detection limit. No Ti^{3+} species were observed in XPS. The absence of peak broadening of Ti $2p_{3/2}$ signals (FWHM was about 1.4 eV for all samples) may also indicate the presence of Ti^{4+} species only [32], and good crystallization for all samples [33]. Figure 5b shows the O 1s core level spectra of pure and doped TiO_2. The peak at 530.1 eV for all samples is due to O^{2-} ion in the TiO_2 lattice. In all spectra at higher binding energy a shoulder is observed (the spectrum of 10% Fe–TiO_2 shows a second peak located at a binding energy of 532.6 eV), which can be attributed to the surface hydroxyl groups of chemisorbed water molecules on the titania [33, 34] or this is the way in which presence of Fe ions influences the TiO_2 matrix. The atomic weight ratio of O to Ti in samples increases with doping: from pure TiO_2: 1.955; 10% Fe-TiO_2: 2.3; to 20% Fe-TiO_2: 3. The XPS spectrum of Fe is very weak (Fig. 5c) due to the low doping level. The presence of Fe ions was detected only in 20% Fe–TiO_2 sample, estimated concentration being about 0.2%. The Fe ions could not be detected in 10% Fe–TiO_2 due to detection limit of instrument, but their presence can be indirectly assumed from O/Ti ratio (2.3), as mentioned before. The binding energies from 711.0 to 711.8 eV and from 725.4 to 726.0 eV should be assigned to $2p_{3/2}$ and $2p_{1/2}$ of Fe^{3+}, respectively. These data exhibit a small shift

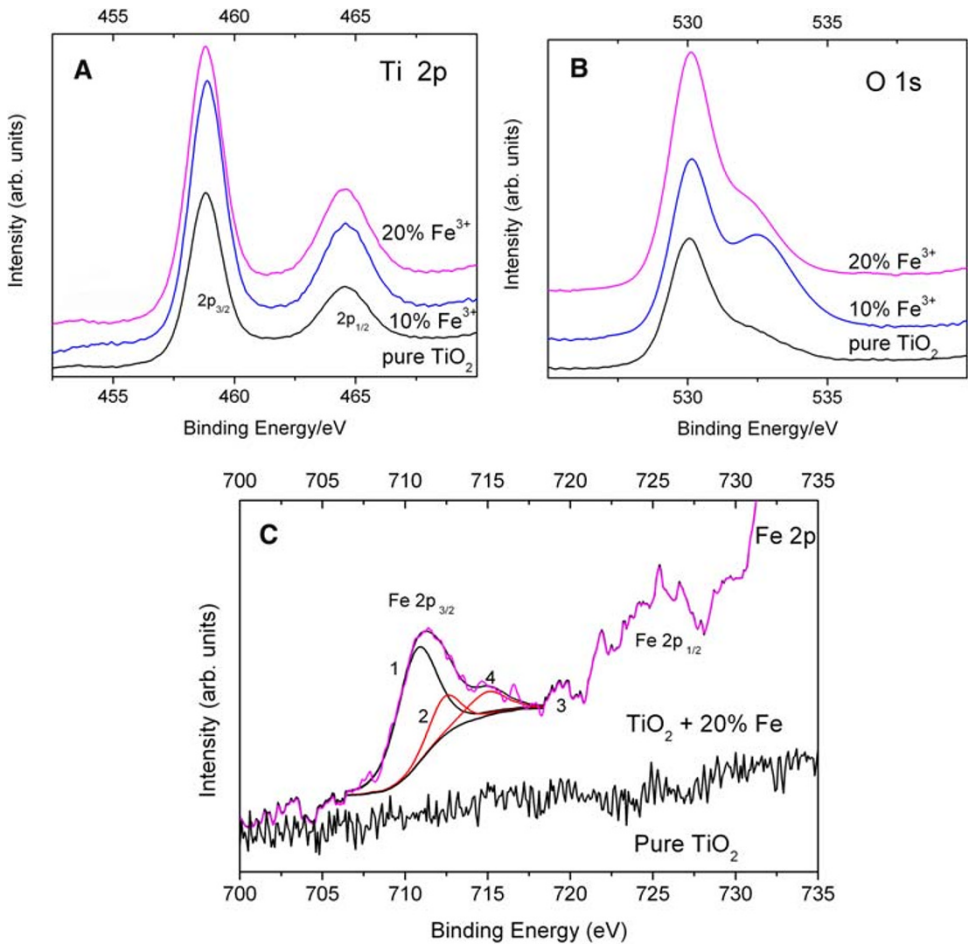

Fig. 5 XPS spectra of pure and doped TiO_2 samples: Ti 2p energy region (**a**), O 1s energy region (**b**), and Fe 2p energy region together with deconvolution of the Fe $2p_{3/2}$ (**c**)

compared to those in Fe_2O_3 (711.3 eV for $2p_{3/2}$) probably indicative of more positively charged surface due to diffusion of the Fe^{3+} in TiO_2 lattice and possible formation of the Fe–O–Ti bond in the sample [35]. Also it can be seen in Fig. 5c that Fe $2p_{3/2}$ peak can be decomposed in several contributions corresponding to different oxidation states of iron. The main contribution can be attributed to Fe^{3+} ions (peak 1, binding energy at 710.9 eV) and the other to Fe^{2+} ions (peak 2, binding energy at 712.8 eV). These statements can be supported with the presence of characteristic satellite peaks at ~720 eV for Fe^{3+} (peak 3) and at ~716 eV for for Fe^{+2} (peak 4), well established for Fe 2p spectra for Fe_2O_3 and FeO, respectively [36].

Concentration of Fe ions in TiO_2 matrix was also checked by emission spectroscopy using ICP instrument. Measurements confirmed that real concentration of Fe in TiO_2 matrix is much lower compared to stoichiometric values, as can be seen in Table 1.

Influence of doping on UV/Vis spectral properties of TiO_2 is clearly evident in Fig. 6, and it is manifested by change of the color of doped powders from light to dark yellow. Reflection spectra of all doped samples contain shoulder at 500 nm, with intensity increasing with Fe^{3+} concentration [31]. Pure TiO_2 has sharp decrease of reflection around 420 nm which corresponds to rutile band gap of ~3.0 eV. The band gap energy of doped TiO_2 samples decrease with increasing Fe concentration—from 3 eV for pure TiO_2 to ~2.3 eV for 20 at.% Fe–TiO_2. This indicates that photocatalytic activity of TiO_2 could be probably influenced by Fe-doping.

Table 1 Concentration of Fe in doped TiO_2 powders, determined by ICP-OES

Sample (% Fe–TiO_2)	Fe at.%
0.0	0.03
2.5	0.20
5.0	0.43
10.0	1.00
20.0	1.70

The influence of Fe-doping on intrinsic TiO_2 photocatalytic activity was studied using photocatalytic degradation of mecoprop, under UV light irradiation. The results are presented in Fig. 7 together with results obtained using commercially available Degussa P25 TiO_2. Iron ions can act in different ways with photogenerated charges [37], as

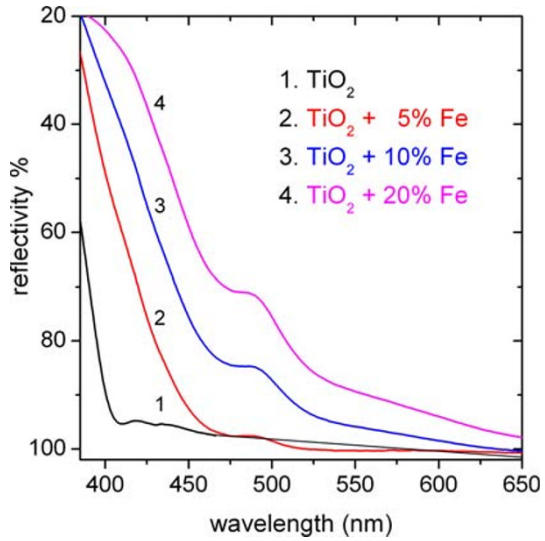

Fig. 6 UV/vis reflectance spectra of pure TiO_2 and TiO_2 doped with different at.% of Fe ions, indicated in the figure

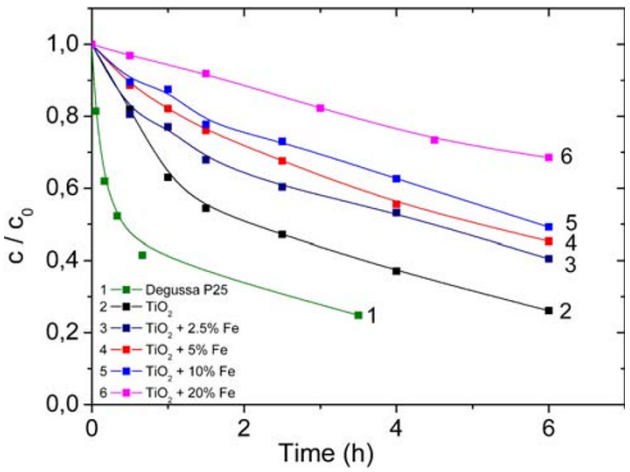

Fig. 7 Kinetics of mecoprop degradation (2.7 mmol dm^{-3}) under UV irradiation monitored by spectrophotometry, in the presence of Fe–TiO_2 with various amounts of Fe ions, pure TiO_2 and Degussa P25 Catalyst amounts: 2 mg cm^{-3}

recombination centre or as charge transfer centre, according to reactions (Eqs. 2–6):

$$TiO_2 + h\nu \rightarrow e_{cb} + h_{vb} \quad (2)$$

$$Fe^{3+} + e_{cb} \rightarrow Fe^{2+} \quad (3)$$

$$Fe^{3+} + h_{vb} \rightarrow Fe^{4+} \quad (4)$$

$$Fe^{4+} + e_{cb} \rightarrow Fe^{3+} \quad (5)$$

$$Fe^{2+} + h_{vb} \rightarrow Fe^{3+} \quad (6)$$

As can be seen in Fig. 7, doping with Fe^{3+} ions reduces photocatalytic activity of degradation of mecoprop. All doped samples showed reduced photocatalytic activity compared to pure rutile and P25 (Table 2). Literature data

Table 2 Effect of at.% Fe in catalysts on mecoprop photocatalytic degradation rate with UV light

Sample (% Fe–TiO_2)	10^3 k' $(min^{-1})^a$	r^b
Degussa P25	0.58	0.855
0.0	0.42	0.995
2.5	0.24	0.966
5.0	0.18	0.993
10.0	0.15	0.973
20.0	0.06	0.999

[a] Pseudo first-order rate constant determined for the first 90 min of irradiation

[b] Linear regression coefficient

concerning influence of Fe doping on TiO_2 photocatalytic activity, showed critical dependence on the method of preparation and choice of compound whose degradation was followed [38–40]. In the case of high doping concentrations, iron ions act mainly as recombination centers for photogenerated electrons (e_{cb}) and holes (h_{vb}) (Eqs. 3–6), the species essential for the production of radicals responsible for mecoprop degradation [24]. As usual, Degussa P25 TiO_2, showed the best photocatalytic activity due to its mixed anatase/rutile phase composition which significantly reduces recombination probability [41].

Doping of TiO_2 with iron ions is also beneficial for introducing oxygen vacancies in/on the crystal lattice or surface of TiO_2 [42]. When oxygen vacancies are on or near the particle surface, they can favor adsorption of water and the formation of surface hydroxyl groups (we have many hydroxyl groups on the surface of samples observed by XPS), which can promote photocatalytic activity. Since it did not happen in our experiments we assumed that oxygen vacancies are mainly inside the nanoparticles. We checked their existence by PL spectra measurements. A typical PL spectra of Fe-doped TiO_2 dispersions (2.5 at.% of Fe), with two different excitation energies, are presented in Fig. 8. One excitation energy is higher than the band gap energy of TiO_2 (4.1 eV) and the other is lower (2.07 eV). In the later case, the observed phenomenon is so called up-conversion (UC)—the observation of an emission at energies higher than the excitation energy [21, 30]. It can be noticed that UC spectra have the same position of peaks/shoulders and similar intensities compared to the normal PL spectrum. Broad emission in the spectral range from 325 to 400 nm was observed as well as the presence of well-resolved peaks/shoulders at 425, 447, 465, 490, and 537 nm.

High energy peaks can be assigned to band edge luminescence of the TiO_2 particles, while lower energy peaks/shoulders are induced by the presence of the oxygen vacancies [21, 30]. Among the other facts, it seems that radiative recombination of photogenerated charge carriers

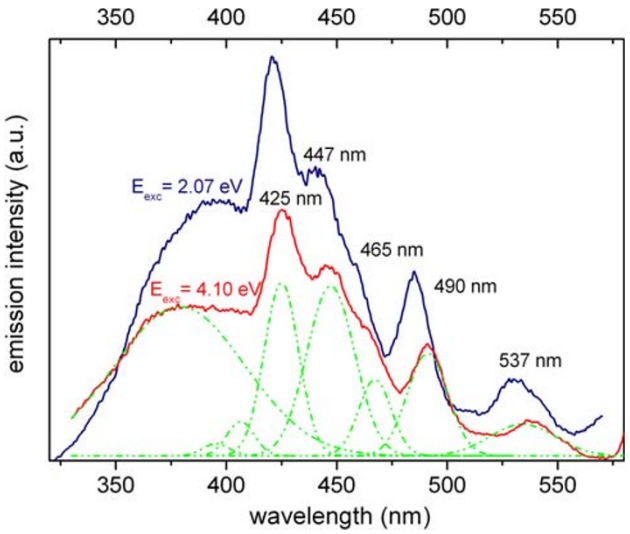

Fig. 8 Typical PL and UCPL spectra and deconvolution of PL spectrum of the rutile 2.5% Fe–TiO_2 nanoparticles

through oxygen vacancy–cascade can also be considered as the process which can decrease the photocatalytic activity of iron doped TiO_2.

Conclusion

TiO_2 nanopowders doped with different concentration of Fe ions were synthesized by coprecipitation method. Applied synthetic procedure induced formation of pure rutile crystalline structure. TEM measurements revealed formation of flower-like agglomerates with diameters in the size range from 100 to 150 nm. XPS measurements showed that Fe ions are mainly in Fe^{3+} oxidation state and that concentrations of incorporated iron ions are much lower than stoichiometric. Doping with Fe ions has great influence on optical characteristics of the host material. Reflection measurements showed that doping of TiO_2 with Fe^{3+} causes shift of the absorption threshold toward visible spectral region. No increase of TiO_2 photocatalytic activity after doping, was observed. The induced photoluminescence as well as the decrease of photocatalytic activity is probably the consequence of the introduction of oxygen vacancies through doping procedure. For higher dopant concentrations (>5%, stoichometric concentration) also recombination of photogenerated charge carriers occurs with higher probability.

Acknowledgments The authors are grateful to Dr Amelia Montone for help in performing SEM measurements. Financial support for this study was granted by the Ministry of Science and Technological Development of the Republic of Serbia (Project No. 142066 and 142029).

References

1. G. Pfaff, P. Reynders, Chem. Rev. **99**, 1963 (1999). doi:10.1021/cr970075u
2. A. Salvador, M.C. Pascual-Marti, J.R. Adell, A. Requeni, J.G. March, J. Pharm. Biomed. Anal. **22**, 301 (2000). doi:10.1016/S0731-7085(99)00286-1
3. R. Zallen, M.P. Moret, Solid State Commun. **137**, 154 (2006)
4. J.H. Braun, A. Baidins, R.E. Marganski, Prog. Org. Coat. **20**, 105 (1992). doi:10.1016/0033-0655(92)80001-D
5. S.A. Yuan, W.H. Chen, S.S. Hu, Mater. Sci. Eng. C **25**, 479 (2005). doi:10.1016/j.msec.2004.12.004
6. A. Fujishima, K. Honda, Nature **37**, 238 (1972)
7. A. Fujishima, T.N. Rao, D.A. Tryk, J. Photochem. Photobiol. Chem. **1**, 1 (2000). doi:10.1016/S1389-5567(00)00002-2
8. D.A. Tryk, A. Fujishima, K. Honda, Electrochim. Acta **45**, 2363 (2000). doi:10.1016/S0013-4686(00)00337-6
9. M. Grätzel, Nature **414**, 338 (2001). doi:10.1038/35104607
10. A. Hagfeldt, M. Grätzel, Chem. Rev. **95**, 49 (1995). doi:10.1021/cr00033a003
11. A.L. Linsebigler, G. Lu, J.T. Yates Jr, Chem. Rev. **95**, 735 (1995). doi:10.1021/cr00035a013
12. A. Millis, S. Le Hunte, J. Photochem. Photobiol. A **108**, 1 (1997). doi:10.1016/S1010-6030(97)00118-4
13. X. Chen, S.S. Mao, Chem. Rev. **107**, 2891 (2007). doi:10.1021/cr0500535
14. A.P. Alivisatos, J. Phys. Chem. **100**, 13226 (1996). doi:10.1021/jp9535506
15. A.P. Alivisatos, Science **271**, 933 (1996). doi:10.1126/science.271.5251.933
16. C. Burda, X. Chen, R. Narayanan, M.A. El-Sayed, Chem. Rev. **105**, 1025 (2005). doi:10.1021/cr030063a
17. C.B. Murray, C.R. Kagan, M.G. Bawendi, Annu. Rev. Mater. Sci. **30**, 545 (2000). doi:10.1146/annurev.matsci.30.1.545
18. Y. Yin, A.P. Alivisatos, Nature **437**, 664 (2005). doi:10.1038/nature04165
19. X. Chen, Y. Lou, S. Dayal, X. Qiu, R. Krolicki, C. Burda, C. Zhao, J. Becker, J. Nanosci. Nanotechnol. **5**, 1408 (2005)
20. U. Diebold, Surf. Sci. Rep. **48**, 53 (2003). doi:10.1016/S0167-5729(02)00100-0
21. N.D. Abazović, M.I. Čomor, M.D. Dramićanin, D.J. Jovanović, S.P. Ahrenkiel, J.M. Nedeljković, J. Phys. Chem. B **110**, 25366 (2006). doi:10.1021/jp064454f
22. Y. Lei, K. Ng, L. Weng, C. Chan, L. Li, Surf. Interface. Anal. **35**, 852 (2003). doi:10.1002/sia.1615
23. A.S. Topalov, D.V. Šojić, D.A. Molnár-Gábor, B.F. Abramović, M.I. Čomor, Appl. Catal. B Environ. **54**, 125 (2004). doi:10.1016/j.apcatb.2004.06.012
24. A. Topalov, D.M. Molnar-Gabor, K.B. Abramovic, Water Res. **34**, 1473 (2000). doi:10.1016/S0043-1354(99)00304-8
25. D. Zhang, L. Qi, J. Ma, H. Cheng, J. Mater. Chem. **12**, 3677 (2002). doi:10.1039/b206996b
26. J. Yang, S. Mei, J.M.F. Ferreira, P. Norby, S. Quaresmâ, J. Colloid Interface Sci. **283**, 102 (2005). doi:10.1016/j.jcis.2004.08.109
27. R. Alexandrescu, F. Dumitrache, I. Morjan, I. Sandu, M. Savoiu, I. Voicu, C. Fleaca, R. Piticescu, Nanotechnology **15**, 537 (2004). doi:10.1088/0957-4484/15/5/023
28. H. Liu, W. Yang, Y. Ma, Y. Cao, J. Yao, J. Zhang, T. Hu, Langmuir **19**, 3001 (2003). doi:10.1021/la026600o
29. L. Miao, S. Tanemura, S. Toh, K. Kaneko, M. Tanemura, Appl. Surf. Sci. **238**, 175 (2004). doi:10.1016/j.apsusc.2004.05.201
30. N.D. Abazović, I.A. Ruvarac-Bugarčić, M.I. Čomor, N. Bibić, S.P. Ahrenkiel, J.M. Nedeljković, Opt. Mater. **30**, 1139 (2008). doi:10.1016/j.optmat.2007.05.038

31. J. Zhu, F. Chen, J. Zhang, H. Chen, M. Anpo, J. Photochem. Photobiol. Chem. **180**, 196 (2006). doi:10.1016/j.jphotochem.2005.10.017
32. W. Zhang, Y. Li, S. Zhu, F. Wang, Chem. Phys. Lett. **373**, 333 (2003). doi:10.1016/S0009-2614(03)00618-3
33. K. Nagaveni, M.S. Hegde, N. Ravishankar, G.N. Subbanna, G. Madras, Langmuir **20**, 2900 (2004). doi:10.1021/la035777v
34. B. Erdem, R.A. Hunsicker, G.W. Simmons, E.D. Sudol, V.L. Dimonie, M.S. El-Aasser, Langmuir **17**, 2664 (2001). doi:10.1021/la0015213
35. A. Glisenti, J. Mol. Catal. A Chem. **153**, 169 (2000). doi:10.1016/S1381-1169(99)00344-1
36. P. Graat, M.A.J. Somers, Appl. Surf. Sci. **100\101**, 36 (1996). doi:10.1016/0169-4332(96)00252-8
37. D. Beydoun, R. Amal, G. Low, S. McEvoy, J. Nanopart. Res. **1**, 439 (1999). doi:10.1023/A:1010044830871
38. C. Wang, C. Böttcher, D.W. Bahnemann, J.K. Dohrmann, J. Mater. Chem. **13**, 2322 (2003). doi:10.1039/b303716a
39. E.P. Reddy, B. Sun, P.G. Smirniotis, J. Phys. Chem. **108**, 17198 (2004). doi:10.1021/jp047419m
40. W.Y. Teoh, R. Amal, L. Mädler, S.E. Pratsinis, Catal. Today **120**, 203 (2007). doi:10.1016/j.cattod.2006.07.049
41. D.C. Hurum, K.A. Gray, T. Rajh, M.C. Thurnauer, J. Phys. Chem. B **109**, 977 (2005). doi:10.1021/jp045395d
42. N. Serpone, J. Phys. Chem. B **110**, 24287 (2006). doi:10.1021/jp065659r